

Cloud optical depth measured with ground-based, uncooled infrared imagers

Joseph A. Shaw*^a, Paul W. Nugent^a, Nathan J. Pust^a, Brian J. Redman^a, Sabino Piazzolla^b

^aElectrical and Computer Engineering Department, Montana State University, Bozeman, Montana, USA 59717; ^bJet Propulsion Laboratory, California Institute of Technology, 4800 Oak Grove Drive, Pasadena, California USA 91109

ABSTRACT

Recent advances in uncooled, low-cost, long-wave infrared imagers provide excellent opportunities for remotely deployed ground-based remote sensing systems. However, the use of these imagers in demanding atmospheric sensing applications requires that careful attention be paid to characterizing and calibrating the system. We have developed and are using several versions of the ground-based "Infrared Cloud Imager (ICI)" instrument to measure spatial and temporal statistics of clouds and cloud optical depth or attenuation for both climate research and Earth-space optical communications path characterization. In this paper we summarize the ICI instruments and calibration methodology, then show ICI-derived cloud optical depths that are validated using a dual-polarization cloud lidar system for thin clouds (optical depth of approximately 4 or less).

Keywords: cloud optical depth, infrared imaging, remote sensing

1. INTRODUCTION

Radiative forcing by aerosols and clouds is a key component of the global climate, and cloud responses to changing aerosols constitute the largest uncertainty in climate modeling.¹ Especially in the Arctic, where satellites have difficulty identifying clouds,² and where the long winter night prevent the year-round use of visible-wavelength, ground-based cloud imagers,^{3,4} there is a need for new remote sensing methods to measure spatial and temporal cloud distributions. The need for improved cloud measurements over a complete diurnal cycle and through the Polar night has been demonstrated using ground-based sensors and satellites.^{3,5-7}

To address this need, as part of a joint U.S.-Japan program to study the Arctic atmosphere, we developed a ground-based, thermal infrared imaging system called the Infrared Cloud Imager (ICI).⁸⁻¹⁰ The ICI method relies on upward-viewing images of downwelling atmospheric emission, recorded with a ground-based thermal infrared imaging system based on an uncooled microbolometer detector array. This allows long-term deployment at remote field sites, but poses significant challenges in establishing and maintaining an accurate radiometric calibration, as such imaging detectors have a response that drifts with the temperature of the focal plane array (FPA). This problem can be dealt with by deploying large-area blackbody sources with the instrument, but this greatly increases the size, weight, and cost of the instrument. Therefore, we developed methods to characterize and compensate for the FPA temperature dependence, thereby enabling long-term radiometric stability and accuracy.¹¹ The 2nd-generation ICI instrument, ICI2, relies on this method to maintain radiometric calibration without an onboard blackbody source. The 3rd-generation ICI instrument, ICI3, uses this method in combination with one onboard blackbody source to achieve even tighter calibration accuracy and stability. These ICI systems record images of long-wave infrared emission from the atmosphere, and allow measurement of spatial and temporal cloud distributions.

An important additional advantage of the ICI technique is that it generates radiometrically calibrated images, which are used to not only identify *cloud presence*, but also *cloud emissivity*⁸ and *cloud optical depth* (OD).¹⁰ Figure 1 shows examples of ICI measurements of (a) atmospheric and cloud radiance, (b) cloud presence, and (c) cloud OD. In the absence of knowledge of the cloud height or temperature, the ICI optical depth algorithm retrieves an upper-limit optical depth for clouds up to OD = 4. The retrieved value comes closer to the actual cloud optical depth as more information is added to the retrieval, most notably cloud height or temperature. In other words, operating the ICI alongside a LIDAR instrument and with a nearby radiosonde allows very accurate retrieval of cloud optical depth at the zenith, with

degraded accuracy at other angles where the actual cloud-base height is unknown. This paper presents a preliminary comparison of the cloud OD values retrieved from the ICI3 instrument with simultaneous LIDAR measurements.

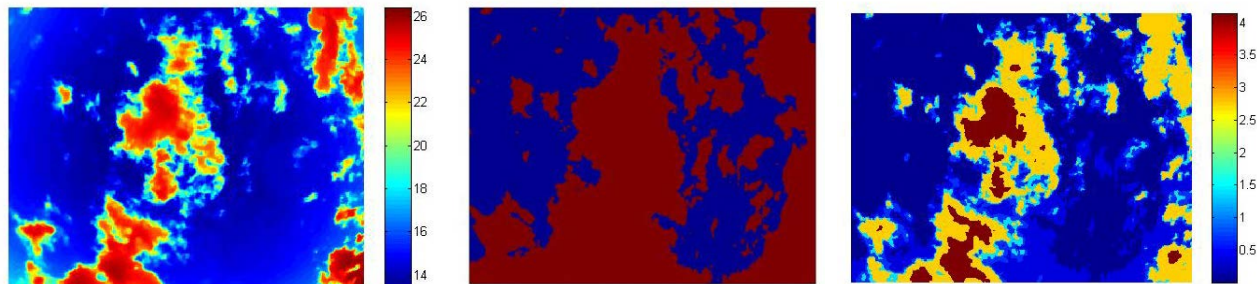


Figure 1. ICI images of (left) radiance [$W/(m^2 sr)$], (center) cloud map (blue=clear, red=cloud), (right) cloud optical depth.

2. METHODOLOGY

Long-wave infrared emission from clouds carries information related to the temperature and emissivity of the clouds, and the emissivity can be related to the OD.^{12,13} Figure 2 shows the relationship between cloud infrared emissivity (ε) and cloud visible optical depth (τ) at $0.55 \mu m$ wavelength, with the dashed line representing the equation proposed by Fu and Liou:¹²

$$\varepsilon = 1 - e^{-0.79\tau}, \quad (1)$$

and the \times symbols representing radiative transfer calculations of infrared emissivity for a database of 4500 real clouds whose heights and optical depths were measured by the Raman lidar at the Atmospheric Radiation Measurements (ARM) Program Southern Great Plains (SGP) site in Lamont, Oklahoma.¹⁴ The radiative transfer calculations were done with MODTRAN4 for the US76 Standard Atmosphere, and the resulting atmospheric emitted spectral radiance was integrated over the ICI spectral response function. The result was a simulation of the spectrally integrated radiance that would be observed by a ground-based, upward-viewing ICI system for the clouds originally observed at the ARM SGP site. Figure 2 demonstrates that equation (1) produces a good prediction of the visible cloud OD from the infrared emissivity (we also note that the visible OD is approximately twice the long-wave infrared OD^{15,16}).

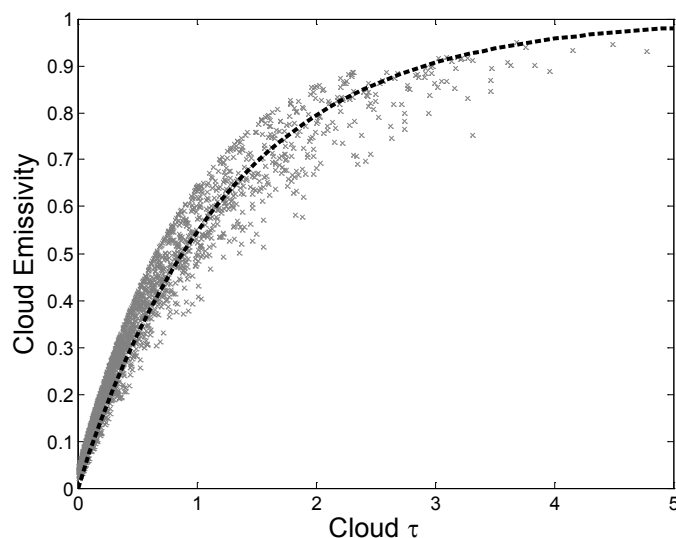


Figure 2. Relationship between infrared cloud emissivity and visible cloud optical depth (τ), with the dashed line representing eq. (1) and the \times symbols representing lidar measurements of visible cloud optical depth at the ARM SGP site.

In the absence of data about cloud height, the ICI algorithm estimates the maximum probable τ for a cloud with a given value of observed radiance. As indicated in Figure 3, the initial version of this algorithm used the MODTRAN4 radiative transfer code with the US76 Standard Atmosphere to simulate the band-averaged radiance that would be observed by a ground-based ICI instrument for the database of approximately 4500 clouds whose heights and optical depths were measured by the Raman Lidar at the ARM SGP site. This resulting database of cloud-radiances was randomly split into a training set and a test set. The training set was used to determine cloud emission thresholds that defined regions where 95% of the clouds had τ less than a specified value. For example, 95% of the clouds in the training set with radiance between 0.86 and 1.29 $\text{W}\cdot\text{m}^{-2}\cdot\text{sr}^{-1}$ had τ less than 0.25, while 95% of the clouds with emission between 0.38 and 0.86 $\text{W}\cdot\text{m}^{-2}\cdot\text{sr}^{-1}$ had τ less than 0.15 (the radiance values used to determine τ have had the non-cloud emission and the atmospheric-path attenuation removed). Unique bins were derived for each month of the year, to capture some of the natural climatological variability. Table 1 lists the maximum likely τ and corresponding radiance thresholds determined from the training set, along with the percentage of clouds from the test set that fell into each band, with the percentage of test clouds that were binned correctly or that had an optical depth higher than the specified maximum value (“% high”). These thresholds can be adjusted to suit a wide range of specific applications or geographic locations.

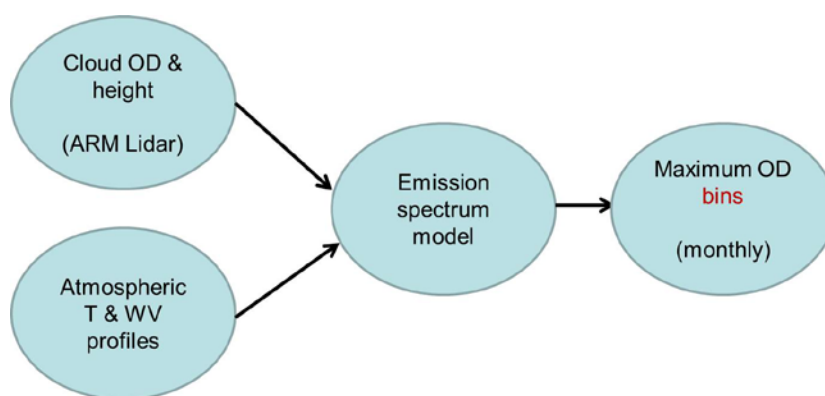


Figure 3. Graphical depiction of the procedure used to estimate the maximum probable cloud optical depth from ICI measurements of cloud radiance in the absence of cloud height information.

Table 1. Visible cloud optical depth (τ) and radiance thresholds

Threshold #	τ	Threshold $\text{W}\cdot\text{m}^{-2}\cdot\text{sr}^{-1}$	% of test clouds	% correct	% high
1	$\tau < 0.06$	0.38	14%	94%	6%
2	$\tau < 0.15$	0.86	17%	95%	5%
3	$\tau < 0.25$	1.29	14%	97%	3%
4	$\tau < 0.50$	2.45	20%	94%	6%
5	$\tau < 1.0$	3.89	18%	94%	6%
6	$\tau < 2.0$	6.89	13%	97%	3%
7	$\tau < 3.0$	12.5	3%	95%	5%
8	$\tau > 3.0$	> 12.5	1%	NA	NA
Total	--	--	--	95%	5%

Clearly, better accuracy can be obtained if the cloud altitude is either known or estimated with reasonable accuracy. In such a case, we follow the procedure outlined in Figure 4. The ICI radiance (after removal of clear-sky emission and path attenuation) is divided by the attenuation-corrected band-average blackbody radiance calculated at the cloud temperature (determined from the cloud height and either observation-specific radiosonde profiles or a model built from a climatology of radiosonde profiles). The result is the cloud emissivity averaged over the ICI spectral response function. This emissivity value is used with equation (1) to determine the visible cloud optical depth.

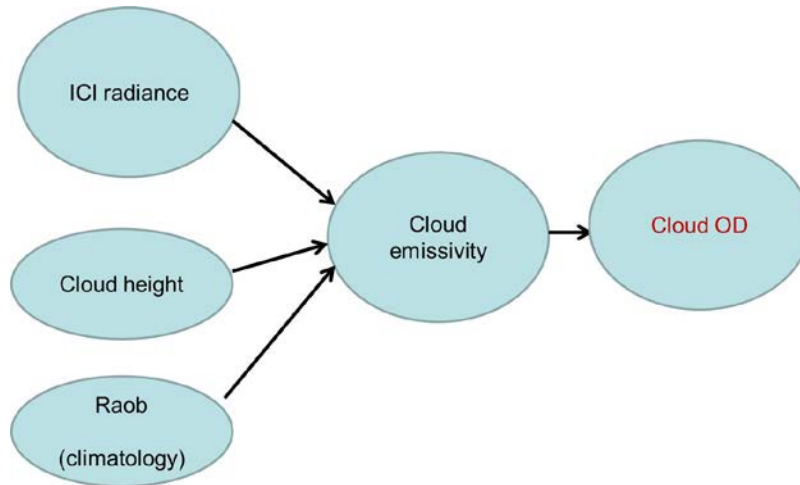


Figure 4. Graphical depiction of the procedure used to estimate the cloud optical depth from ICI measurements of cloud radiance with cloud height information.

As an initial validation of the ICI cloud optical depth retrievals, ICI data were compared with cloud optical depth estimates from the Montana State University dual-polarization lidar system.¹⁷ Lidar data were processed using two methods to extract the cloud optical depth^{18,19} Method 1¹⁸ used MODTRAN and an iterative process and worked well for clouds with an optical depth less than approximately 2, but often did not converge for optically thicker clouds. Method 2¹⁹ used a ratio of lidar backscatter measurements above and below the cloud and worked well for clouds with an optical depth greater than 1 (when cloud boundaries are well determined). In the overlap region where the two methods both work well, they produced values with greater than 90% agreement.

3. RESULTS

The procedures outlined in the previous section were used to retrieve cloud optical depth from ICI measurements made at Bozeman, Montana, during the spring and summer of 2010. The zenith ICI cloud optical depth values were compared with simultaneous lidar measurements. Figure 5 shows results of such a comparison using the ICI algorithm that did not incorporate cloud height information. The lidar data were temporally averaged for a 10 second window when the ICI data were present, and the ICI data were spatially averaged over a 1° field of view centered on the zenith. As expected, the absolute agreement was not so good, but it was encouraging that the ICI retrievals of maximum-probable optical depth were above the more direct lidar measurements 92.2% of the time.

Figure 6 shows results of a comparison using the ICI algorithm that incorporated cloud height measured by the lidar, along with an actual surface air temperature value and a monthly atmospheric profile model derived from radiosondes launched by us at Montana State University over a four-year period (i.e., we did not use radiosonde data specific to each cloud measurement). In this comparison, the lidar data were averaged from the results of the two lidar retrieval methods, but when either algorithm did not produce a good result, data from only one lidar retrieval method were used. In all cases, the lidar and ICI data were temporally averaged over a 5-minute period. These data exhibit a correlation

coefficient of 0.89, a root mean square (rms) error of 0.21 optical depth, and a mean error of 0.041 optical depth. These promising results are plotted as a histogram of the difference of the ICI and lidar optical depths in Figure 7.

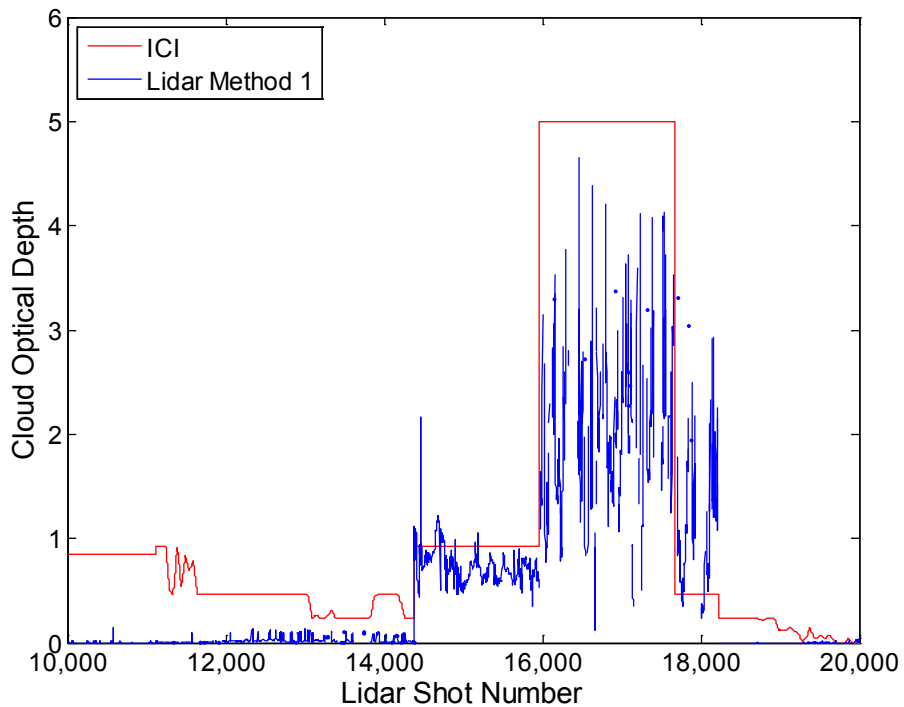


Figure 5. Comparison of maximum-probable cloud optical depth retrieved from the ICI (blue line) and lidar-derived cloud optical depth (red line) for a variety of non-sequential observations at Bozeman, Montana during 2010.

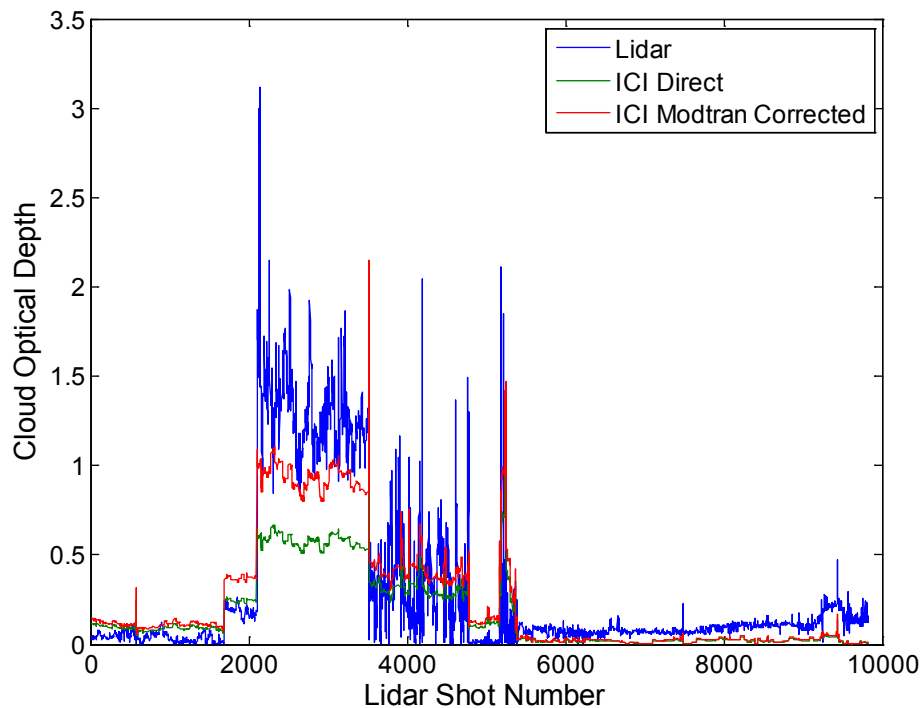


Figure 6. Comparison of cloud optical depth retrieved from the ICI using the lidar-measured cloud height (blue line) and lidar-derived cloud optical depth (red line) for a variety of non-sequential observations at Bozeman, Montana during 2010.

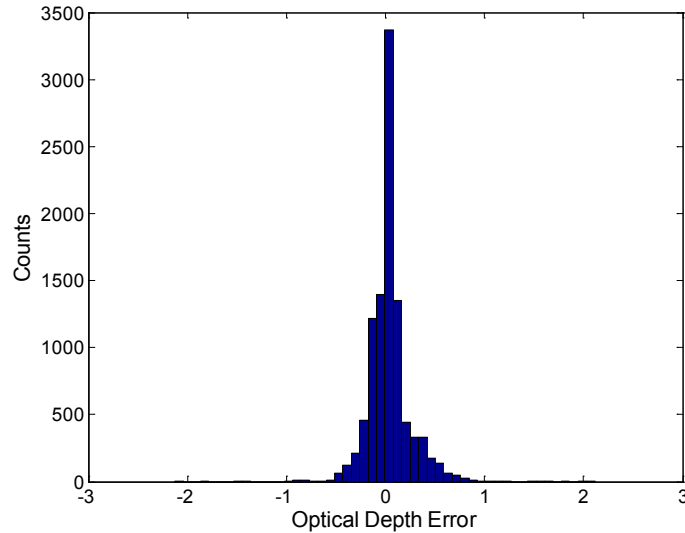


Figure 3. Histogram of the difference between ICI and lidar cloud optical depth for the data shown in Figure 6.

4. CONCLUSIONS

The ICI method can retrieve a maximum-probable cloud optical depth with modest accuracy in the absence of cloud height information (only 6% of test clouds had an actual optical depth higher than the ICI-derived maximum-probable optical depth). When lidar-derived cloud height was incorporated into a seasonal atmospheric model, ICI measurements agreed with lidar measurements of cloud optical depth to within ± 0.21 optical depth units, with a small bias of 0.04. Future work is focusing on additional refinement of the ICI retrieval algorithms, and more complete validation with an extended data set.

Acknowledgments.

Portions of this research were carried out at the Jet Propulsion Laboratory, California Institute of Technology, under a contract with the National Aeronautics and Space Administration.

5. REFERENCES

- [1] IPCC, "Climate Change 2007: Synthesis Report," Intergovernmental Panel on Climate Change, http://www.ipcc.ch/publications_and_data/ar4/syr/en/contents.html (2007).
- [2] M. S. Town, V. P. Walden, and S. G. Warren, "Cloud cover over the South Pole from visual observations, satellite retrievals, and surface-based infrared radiation measurements," *J. Clim.*, **20**(3), 544-559 (2007).
- [3] E. L. Key, P. J. Minnett, R. A. Jones, "Cloud distributions over the coastal Arctic Ocean: surface-based and satellite observations," *Atmos. Res.*, **72**, 57-88 (2004).
- [4] C. N. Long, J. M. Sabburg, J. Calbo, and D. Pages, "Retrieving cloud characteristics from ground-based daytime color all-sky images," *J. Atmos. Ocean. Technol.*, **23**(5), 633-652 (2006).

- [5] R. G. Ellingson and M. B. Ba, "A study of diurnal variation of OLR from the GOES Sounder," *J. Atmos. Ocean. Technol.*, **20**, 90-98 (2003).
- [6] M. A. Miller, M. P. Jensen, and E. E. Clothiaux, "Diurnal cloud and thermodynamic variations in the stratocumulus transition regime: A case study using in situ and remote sensors," *J. Atmos. Sci.*, **55**, 2294-2310 (1998).
- [7] P. Minnis, D. R. Doelling, V. Chakrapani, D. A. Spangenberg, L. Nguyen, R. Palikonda, T. Uttal, R. F. Arduini, and M. Shupe, "Cloud Coverage During FIRE ACE Derived from AVHRR Data," *J. Geophys. Res.* **106**, 15,215-15,233 (2001).
- [8] J. A. Shaw, P. W. Nugent, N. J. Pust, B. Thurairajah, and K. Mizutani, "Radiometric cloud imaging with an uncooled microbolometer thermal infrared camera," *OpEx*, 13(15), 5807-5817 (2005).
- [9] B. Thurairajah and J. A. Shaw, "Cloud statistics measured with the infrared cloud imager," *IEEE Trans. Geosci. Remote Sens.*, 43(9) 2000-2007 (2005).
- [10] P. W. Nugent, J. A. Shaw, and S. Piazzolla, "Infrared cloud imaging in support of Earth-space optical communication," *Opt. Eng.*, 17(10), 7862-7872 (2009).
- [11] P. W. Nugent, J. A. Shaw, and N. J. Pust, "Correcting for focal plane array temperature dependence in microbolometer infrared cameras lacking thermal stabilization," *Opt. Eng.* (in press, Nov. 2012).
- [12] Q. Fu and K. N. Liou, "Parameterization of the radiative properties of cirrus clouds," *J. Atmos. Sci.*, 50(13), 2008-2025 (1993).
- [13] K. Sassen and G. G. Mace, "ground-based remote sensing of cirrus clouds," in *Cirrus*, D. K. Lynch, K. Sassen, D. O'C. Starr, and G. Stephens, eds (Oxford, New York, NY), 168-209 (2002).
- [14] T. P. Ackerman and G. Stokes, "The Atmospheric Radiation Measurement Program," *Physics Today*, **56**, 38-45 (2003).
- [15] D. H. DeSlover, W. L. Smith, P. K. Piironen, and E. W. Eloranta, "A methodology for measuring cirrus cloud visible-to-infrared spectral optical depth ratios," *J. Atmos. Oceanic Technol.*, **16**, 251-262 (1999).
- [16] C. M. R. Platt, J. C. Scott, and A. C. Dilley, "Remote sounding of high clouds. Part VI: Optical properties of midlatitude and tropical cirrus," *J. Atmos. Sci.*, **44**, 729-747 (1987).
- [17] N. L. Seldomridge, J. A. Shaw, and K. S. Repasky, "Dual-polarization lidar using a liquid crystal variable retarder," *Opt. Eng.*, **45**(10), 106202 (2006).
- [18] S. A. Young, "Analysis of lidar backscatter profiles in optically thin clouds," *Appl. Opt.*, **44**(30), 7019-7031 (1995).
- [19] C. S. Cook, G. W. Bethke, and W. D. Conner, "Remote measurement of smoke plume transmittance using lidar," *Appl. Opt.*, **11**(8), 1742-1748 (1972).